Notochord vacuoles are lysosome-related organelles that function in axis and spine morphogenesis

Kathryn Ellis, Jennifer Bagwell, and Michel Bagnat

Department of Cell Biology, Duke University Medical Center, Durham, NC 27710

The notochord plays critical structural and signaling roles during vertebrate development. At the center of the vertebrate notochord is a large fluid-filled organelle, the notochord vacuole. Although these highly conserved intracellular structures have been described for decades, little is known about the molecular mechanisms involved in their biogenesis and maintenance. Here we show that zebrafish notochord vacuoles are specialized lysosome-related organelles whose formation and maintenance requires late endosomal trafficking regulated by the vacuole-specific Rab32a and H^+-ATPase–dependent acidification. We establish that notochord vacuoles are required for body axis elongation during embryonic development and identify a novel role in spine morphogenesis. Thus, the vertebrate notochord plays important structural roles beyond early development.

Introduction

The acquisition of a notochord is an important event in evolutionary history as it marks the beginning of our phylum, Chordata. In vertebrates, the notochord arises from the dorsal organizer, also known as the embryonic shield in zebrafish, and is critical for proper vertebrate development (Shih and Fraser, 1996; Saúde et al., 2000). It persists throughout life in nonvertebrate chordates and in vertebrates contributes to the nucleus pulposus of intervertebral discs (Hunter et al., 2004; Choi et al., 2012; McCann et al., 2012). The notochord is also an important midline structure that serves both patterning and structural roles during the early gastrula period.

In zebrafish, the notochord is one of the earliest distinguishable features in the embryo. It forms as chordamesoderm cells converge at the midline and intercalate, creating a rod of stacked cells with a characteristic "stack of coins" appearance (Glickman et al., 2003; Sepich et al., 2005). Around the 15 somite stage (15 ss) or 16.5 h post-fertilization (hpf) this stack of cells differentiates into two distinct cell populations in a notch-dependent manner (Yamamoto et al., 2010)—the outer sheath layer, previously referred to as chordoblasts (Grotmol et al., 2003) or notochord sheath cells (Dale and Topczewski, 2011), and an inner vacuolated cell layer, previously referred to as chordocytes (Grotmol et al., 2003). The outer cells secrete a thick extracellular perinotochordal basement membrane, whereas the inner cells form large fluid-filled intracellular vacuoles. The vacuoles occupy the majority of the volume of the inner cells with diameters of up to 40 µm. Notochord vacuoles have been described in nearly every embryonic vertebrate studied from fish to amphibians, birds, and mammals (Leeson and Leeson, 1958; Waddington and Perry, 1962; Bancroft and Bellairs, 1976). In these species the vacuoles are maintained in the cells of the nucleus pulposus where they persist well beyond skeletal maturity (Meachim and Cornah, 1970; Hunter et al., 2004).

The notochord is also a source of developmental signals that pattern surrounding tissue including the neural tube (Yamada et al., 1991, 1993), somites (Pourquié et al., 1993; Schmidt et al., 1995; Griffin and Kimelman, 2003), blood vessels (Fouquet et al., 1997), and the pancreas (Kim et al., 1997). Structurally, the notochord acts as a hydrostatic skeleton for the embryo before bone formation. This axial support is crucial for locomotion in embryos that develop externally, such as fish and amphibians, to evade predation. The pressure exerted from the inflating notochord vacuoles on the constricting perinotochordal basement membrane gives this structure its flexural stiffness and mechanical strength (Koehl et al., 2000). Notochords dissected from *Xenopus laevis* embryos are osmotically

Correspondence to Michel Bagnat: m.bagnat@cellbio.duke.edu

Abbreviations used in this paper: BFA, brefeldin A; DIC, differential interference contrast; DN, dominant-negative; dpf, days post-fertilization; GAG, glycosaminoglycan; hpf, hours post-fertilization; LRO, lysosome-related organelle; MED, methyl ester dye; NICD, notch intracellular domain; ss, somite stage; UAS, upstream activating sequence; VPS, vacuolar protein sorting; WT, wild type.

The Rockefeller University Press $30.00
J. Cell Biol. Vol. 200 No. 5 667–679
www.jcb.org/cgi/doi/10.1083/jcb.201212095

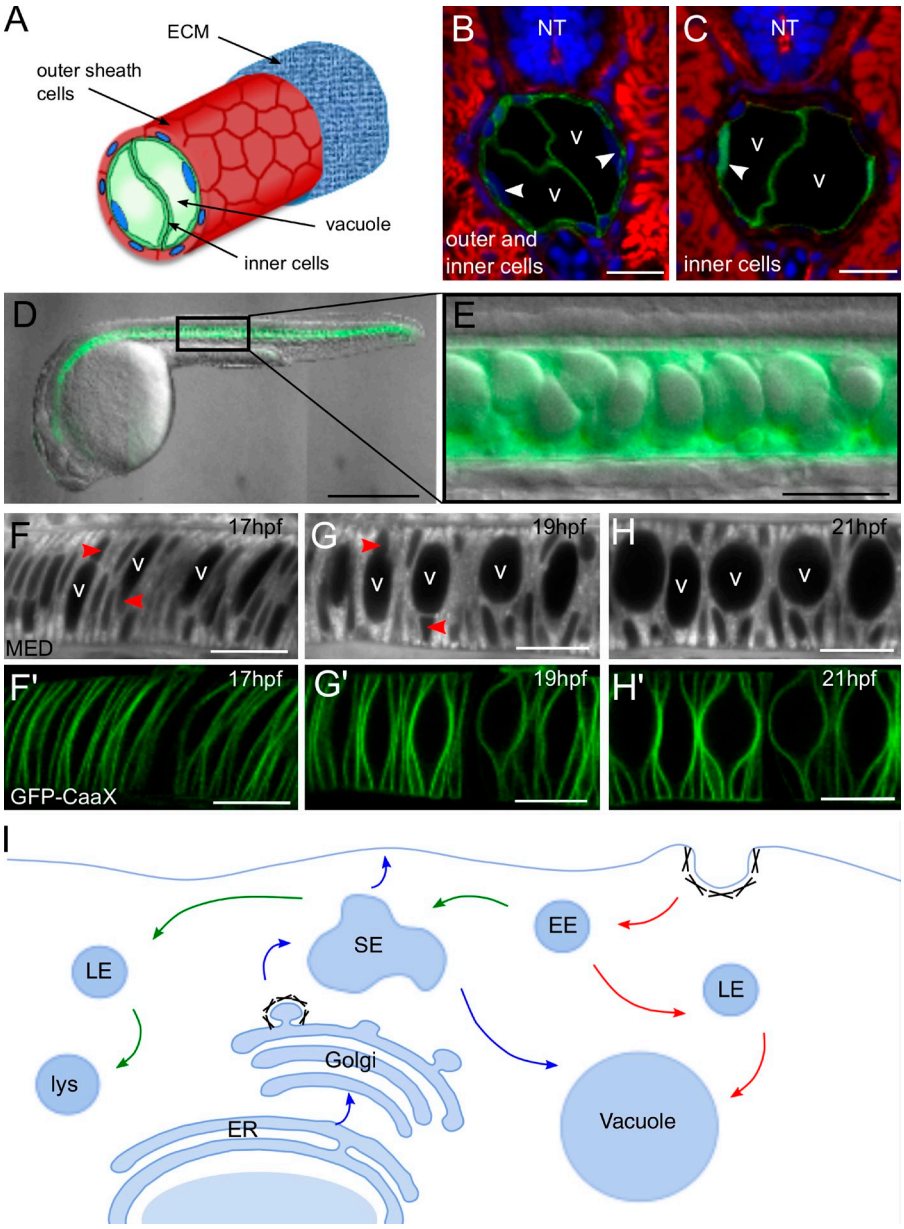

Figure 1. **Zebrafish notochords contain intracellular vacuoles that inflate rapidly during development.** (A) Cartoon of a zebrafish notochord depicting outer and inner cell layers and the inner cell vacuoles. (B) Confocal image of a cross section of 3-dpf transgenic larva labeled with membrane GFP (GFP-CaaX) in the outer and inner cells (*Tg(rcn3:GFP-CaaX)*). (C) Confocal image of a cross section of a 3 dpf transgenic larva expressing soluble GFP in the inner cells (*Gt(SAGFF214A:gal4); Tg(UAS:GFP)*). Cross sections were stained with phalloidin in red and DAPI in blue. V, vacuole; NT, neural tube; arrowheads show inner cell nuclei. (D) 24-hpf transgenic GFP-CaaX embryo illustrating orientation of fish for all live imaging done in this work (*Tg(rcn3:GFP-CaaX)*). Anterior is left, posterior is right, dorsal is top, and ventral is bottom. (E) DIC image of 24-hpf GFP-Caax embryo showing approximate position along anterior-posterior axis where all images were acquired. (F–H′) WT vacuole inflation was visualized with the vital dye BODIPY TR MED using live confocal time-lapse imaging of GFP-CaaX transgenic embryos—*Tg(rcn3:gal4); Tg(UAS:GFP-CaaX)*. v, vacuole; arrowheads show nuclei. (I) Cartoon depicting possible trafficking routes to the vacuole. Red arrows indicate endocytic traffic, blue arrows indicate biosynthetic traffic, and green arrows indicate lysosomal degradation pathway. EE, early endosome; LE, late endosome; SE, sorting endosome; lys, lysosome. Bars: (B and C) 20 µm; (D) 500 µm; (E–H) 50 µm.

active structures and undergo drastic shape changes in hypotonic and hypertonic conditions (Adams et al., 1990). Similarly, osmotic activity was also seen in dissociated cells from canine intervertebral discs (Hunter et al., 2007). It has been suggested that the pressure generated within the notochord from the inflating vacuoles acts as a morphogenic force that elongates and straightens the embryo along the anterior-posterior axis (Adams et al., 1990; Koehl et al., 2000). However, this has only been shown ex vivo and in modeled notochords and in vivo data supporting this model is still lacking.

Notochord vacuoles have been described for decades, yet the molecular mechanisms involved in their formation and their function during development remain unknown. Here we show that notochord vacuoles are specialized post-Golgi structures whose biogenesis and maintenance require late endosomal trafficking regulated by *rab32a* and H^+-ATPase–dependent acidification. These characteristics together with the presence of a lysosomal membrane protein led us to conclude that notochord vacuoles are unique lysosome-related organelles (LROs). By disrupting vacuolated cell differentiation or integrity, we reveal a critical role for notochord vacuoles in embryonic body axis elongation and spine morphogenesis.

Results

Biosynthetic trafficking is required for the rapid inflation of notochord vacuoles

The zebrafish notochord is comprised of two cell layers, an outer epithelial-like sheath and an inner layer of cells containing one large vacuole each that occupies the majority of the cell volume (Fig. 1 A). To elucidate how notochord vacuoles are formed we generated various transgenic zebrafish lines to drive notochord-specific or inner cell–specific expression of various transgenes. To drive expression in both outer and inner

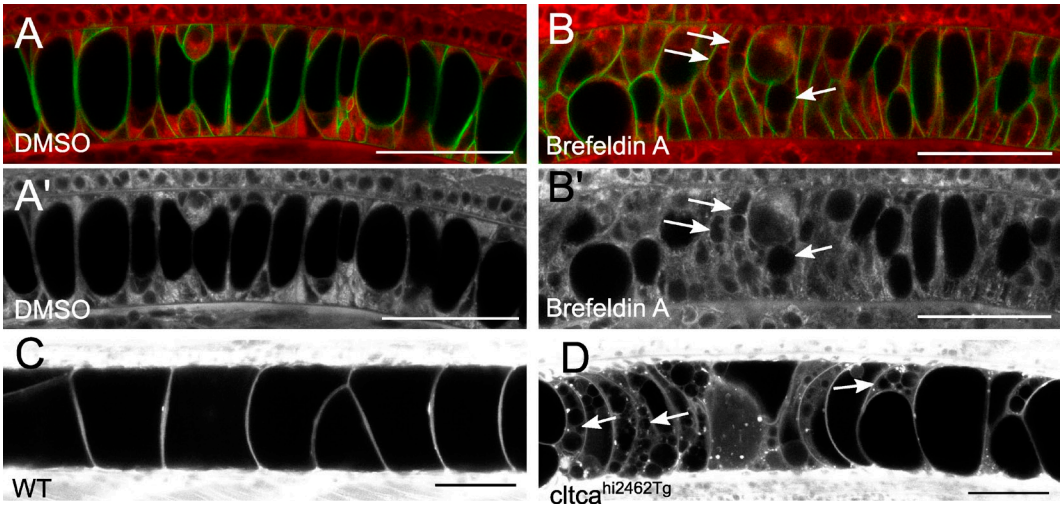

Figure 2. **Biosynthesis is required for notochord vacuole biogenesis.** (A–B′) Live confocal images of embryos treated with either DMSO or 5 µg/ml BFA at the time of vacuole inflation and visualized with membrane GFP and MED merge (A and B) or MED alone (A′ and B′). Arrows label fragmented or small vacuoles. (C and D) Live confocal image of *cltca*^{hi2462Tg} mutant and WT sibling larvae at 4 dpf dyed with MED. Arrows label fragmented or small vacuoles. Bars, 50 µm.

cell populations we isolated an ∼1-kb regulatory sequence from the *rcn3* gene (Fig. 1 B). This promoter sequence is active in the notochord before vacuole formation, beginning at 6 ss (∼12 hpf; Fig. S1). For inner cell–specific expression we used a gal4 enhancer trap line (SAGFF214A) that is active after vacuole formation at 26 ss (∼22 hpf; Yamamoto et al., 2010; Fig. 1 C).

To determine the time course of notochord vacuole formation we first performed live, time-lapse imaging of vacuole expansion in wild-type (WT) embryos. All live imaging in this work was performed in the same orientation at approximately the same position along the anterior-posterior axis (Fig. 1, D and E). Transgenic membrane GFP (GFP-CaaX) embryos were incubated in the vital dye BODIPY TR methyl ester dye (MED) to visualize internal membranes (Fig. 1, F–H). We observed that over the course of 4 h (from 17 to 21 hpf) notochord vacuoles expand their volume dramatically, changing the shape of the prospective inner cells from disc-shaped rods to large spheroids. Concurrently, outer cells migrate to the periphery to form an epithelial-like sheath surrounding the inner cells (Dale and Topczewski, 2011).

There are several trafficking routes that could contribute membrane and cargo to the growing vacuole (Fig. 1 I). Vacuoles could receive contributions from endocytic trafficking via endosomes, biosynthetic trafficking through the ER and Golgi complex, or both.

To determine if biosynthetic trafficking contributes to the growing vacuole membrane, embryos were treated with brefeldin A (BFA), an inhibitor of ER to Golgi transport (Lippincott-Schwartz et al., 1989). Notochord-specific GFP-CaaX embryos were treated before vacuole formation for a period of 5 h from 16 until 25 ss with either 5 µg/ml BFA or DMSO. Although vacuole formation initiated and progressed normally in DMSO-treated embryos, the vacuoles failed to inflate in BFA-treated embryos (Fig. 2, A and B), indicating that ER to Golgi trafficking is essential for vacuole biogenesis. This role for ER to Golgi transport is consistent with the defects seen in the notochords of COPI and COPII mutant zebrafish (Odenthal et al., 1996; Stemple et al., 1996; Coutinho et al., 2004; Melville et al., 2011).

Next, to investigate the potential role of post-Golgi trafficking in vacuole formation we asked whether clathrin coats are required. Clathrin coats are important mediators of coated vesicle formation in post-Golgi trafficking as well as during plasma membrane internalization from the cell surface (Anderson et al., 1977; Deborde et al., 2008). The transgenic line *cltca*^{hi2462Tg} contains a retroviral insertion in the clathrin heavy chain gene, which generates a null mutant allele (Amsterdam et al., 2004). Using live confocal imaging we observed that in clathrin mutants, but not in WT siblings, notochord vacuoles begin to fragment and fall apart around 96 hpf (Fig. 2, C and D). This phenotype is not apparent until 4 days post-fertilization (dpf), most likely because of a maternal load of functional protein. This data implicates post-Golgi trafficking in vacuole maintenance.

We next investigated the presence of secreted cargo within the vacuole lumen. We generated secreted versions of GFP and RFP and tested them for secretion in vitro (Fig. S2 A). In transgenic embryos expressing secreted GFP in the notochord, no GFP was detected in the lumen of the vacuole (Fig. S2 B). Because bulk secretory cargo is sorted away from the vacuole, our data suggest that a specialized post-Golgi trafficking pathway is required for notochord vacuole biogenesis.

Endocytosis is not a major contributor to vacuole formation or maintenance

Because clathrin is involved in vesicle formation at both the Golgi complex and the plasma membrane during endocytosis, we next investigated if endocytosis contributes to the growing vacuole. To determine whether endocytosis is required for vacuole formation we generated dominant-negative (DN) constructs to block dynamin, a GTPase that plays a major role in endocytosis as well as in Golgi complex exit (Chen et al.,

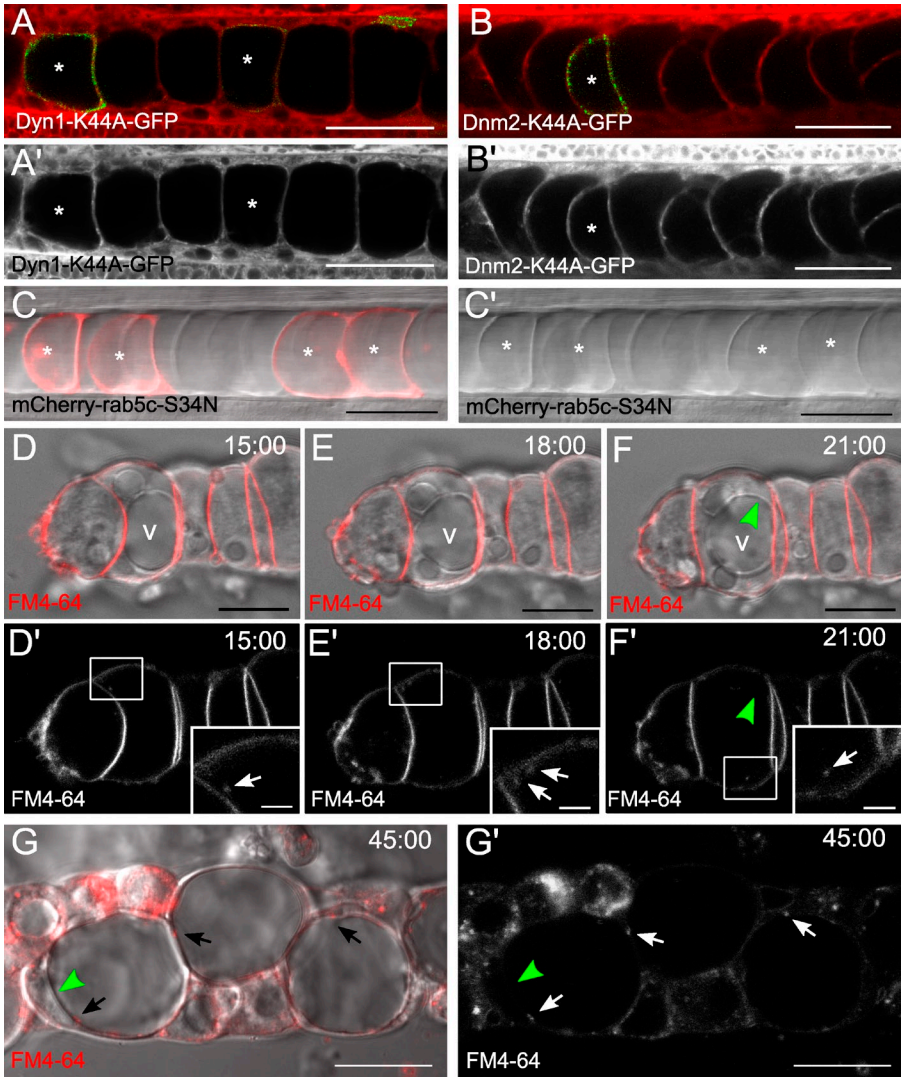

Figure 3. **Endocytosis is not a major contributor to vacuole formation or maintenance.** UAS:Dyn1-K44A-GFP and UAS:Dyn2-K44A-GFP DNA were injected into *Tg(rcn3:gal4)* embryos for mosaic expression of DN dynamin1 or dynamin2. (A) Live confocal image of a 24-hpf embryo mosaically expressing DN dynamin1-GFP and stained with MED. Asterisks mark expressing cells. (A′) MED alone. (B) Live confocal image of a 24-hpf embryo mosaically expressing DN dynamin2-GFP and stained with MED. Asterisks mark expressing cells. (B′) MED alone. (C) Live confocal image of a 48-hpf embryo expressing DN mCherry-Rab5 in the inner cells (*Gt(SAGFF214A:gal4); Tg(UAS:mCherry-rab5c-S34N)*). Asterisks mark expressing cells. (C′) DIC alone. (D–F′) Still images from time-lapse confocal live imaging of dissected notochords cultured with FM4-64. Bright field and FM4-64 dye merged (D–F) and FM4-64 dye in grayscale alone (D′–F′) are shown. Arrows indicate FM4-64–labeled endosomes in inner cells. v, vacuole. After 20 min, no FM dye is seen on the vacuole membrane (F, green arrowhead). (G) In further dissociated notochords, cells internalize more dye. Arrows indicate FM dye–labeled endosomes in inner cells and green arrowheads label vacuole membrane. Bright field and FM dye merged (G) and FM dye in grayscale alone (G′) are shown. Bars: (A–C) 50 µm; (D–F) 10 µm; (D′–F′, insets) 2 µm; (G) 20 µm.

1991; Herskovits et al., 1993; Kreitzer et al., 2000). DN dynamin constructs were expressed mosaically or induced after notochord differentiation to avoid defects in convergent extension and differentiation of the outer and inner cell types (Kida et al., 2007). Upstream activating sequence (UAS):Dyn1-K44A-GFP or UAS:Dyn2-K44A-GFP DNA were injected into *Tg(rcn3:gal4)* embryos at the one-cell stage and embryos were then live imaged at 24 hpf using confocal microscopy. We observed that most inner cells expressing DN dynamin had fully inflated vacuoles, whereas only 9.6% of expressing cells had fragmented vacuoles ($n = 52$ cells; Fig. 3, A and B).

We also tested the requirement of endocytosis for vacuole maintenance by expressing a DN version of the early endosome regulator Rab5c. To drive the expression of DN Rab5c after vacuole formation we crossed the SAG214A driver described previously to a *Tg(UAS:mCherry-rab5c-S34N)* line (Yamamoto et al., 2010; Clark et al., 2011). At 2 dpf, when the DN protein had been present in the inner cells for at least 24 h, transgenic embryos had normal notochords with fully inflated vacuoles (Fig. 3 C). Of the inner cells expressing DN Rab5c, only 2.8% were fragmented at 2 dpf ($n = 572$ cells), suggesting that early endosome trafficking is not required for vacuole maintenance.

To test more directly the contribution of endocytosis to vacuole formation we used the endocytic tracer FM4-64 to track internalized membranes. Because FM4-64 did not readily label inner notochord cells in intact embryos, we cultured dissected notochords in medium with FM4-64 for 30 min and then assessed dye distribution by confocal microscopy. In partially intact notochords, the dye was internalized and transiently colocalized with the early endosomal marker Venus-FYVE (unpublished data). However, there was little internalization of the dye and few detectable endosomes in the inner cells after 1 h, and no FM4-64 was seen on the vacuole membrane (Fig. 3, D–F). To enhance endocytosis we dissociated notochords further and incubated them with dye for 20 min. After washing out unincorporated dye, we added fresh media and monitored the notochord cells for an additional 40 min using confocal microscopy. Under these conditions much more FM4-64 was internalized, yet the dye never labeled the vacuole membrane (Fig. 3 G). Similar experiments were also done with fluorescently labeled dextran. After incubation for 30 min, dextran-labeled punctae were seen within cells but no dextran was visible inside the vacuole (unpublished data). Collectively, these data show that notochord vacuoles do not

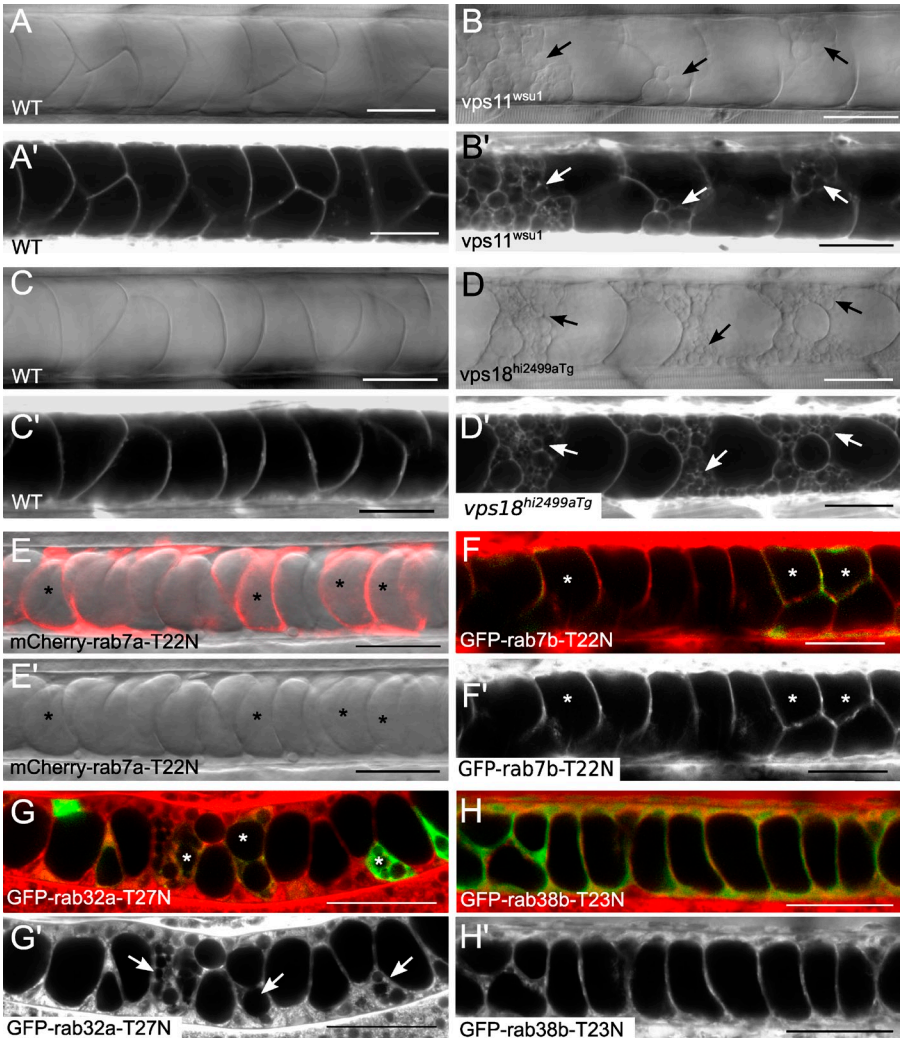

Figure 4. **Vacuole formation requires late endosomal machinery and the vacuole-specific rab32a.** (A and A′) Live DIC and confocal images of a 3-dpf WT sibling. (B and B′) Live DIC and confocal images of a 3-dpf *vps11*^{wsu1} mutant larva dyed with MED. Arrows indicate fragmented vacuoles. (C and C′) Live DIC and confocal images of a 3 dpf WT sibling. (D and D′) Live DIC and confocal images of a 3-dpf *vps18*^{hi2499aTg} mutant larva dyed with MED. Arrows indicate fragmented vacuoles. (E) Live confocal image of a 24-hpf transgenic embryo expressing DN mCherry-Rab7a (*Tg(rcn3:gal4); Tg(UAS:mCherry-rab7a-T22N)*). (E′) DIC alone. Asterisks label expressing cells. (F) UAS:GFP-rab7b-T22N DNA injected into *Tg(rcn3:gal4)* embryos for mosaic expression of DN GFP-Rab7b. Live confocal image of a 24-hpf embryo with MED and GFP merged. (F′) MED in grayscale alone. Asterisks label expressing cells. (G) UAS:GFP-rab32a-T27N DNA injected into *Tg(rcn3:gal4)* embryos for mosaic DN GFP-Rab32a expression. Live confocal image of a 24-hpf embryo with MED and GFP merged. (G′) MED in grayscale alone. Asterisks label expressing cells and arrows indicate fragmented vacuoles. (H) Live confocal image of a 24-hpf transgenic embryo expressing DN GFP-Rab38b in the notochord (*Tg(rcn3:gal4); Tg(UAS:GFP-rab38b-T23N)*). MED and GFP merged (H) and MED in grayscale alone (H′) are shown. Bars, 50 µm.

receive internalized membranes or soluble cargo via endocytosis and that endocytosis does not play a major role in vacuole maintenance.

Vacuole formation requires late endosomal machinery and Rab32a

Clathrin is known to regulate vesicular traffic out of the Golgi complex and, as shown here, is required for vacuole maintenance. To investigate the role of the post-Golgi late endosomal pathway in vacuole formation, we obtained mutant zebrafish with null alleles of genes that function at the late endosome and lysosome, vacuolar protein sorting (VPS) genes. VPS genes were first discovered and characterized in yeast, where they function to regulate the trafficking of transport vesicles to the yeast vacuole (Raymond et al., 1992). Zebrafish mutants for *vps11* and *vps18* were shown to have pigmentation defects in the skin and retinal epithelium as well as liver defects (Sadler et al., 2005; Thomas et al., 2011). Using live confocal and differential interference contrast (DIC) imaging we analyzed the notochords of 2 dpf *vps11*^{wsu1} and *vps18*^{hi2499aTg} mutant embryos and found that notochord vacuoles fragment and appear disorganized in these mutants, indicating that the late endosomal pathway is important for vacuole maintenance (Fig. 4, A–D).

Next, we tested if Rab7, the classical regulator of late endosomes, is important for vacuole formation. To this end we expressed DN mCherry-Rab7a (Clark et al., 2011) under the control of the *rcn3:gal4* driver. Live confocal imaging revealed that inner cells developed vacuoles normally in transgenic embryos expressing DN mCherry-Rab7a in the notochord (Fig. 4 E). As several isoforms of *rab7* exist in zebrafish we also generated and tested the effects of a DN GFP-Rab7b construct. UAS:GFP-rab7b-T22N DNA was injected into *Tg(rcn3:gal4)* embryos at the one-cell stage. At 24 hpf, mosaic expression of DN GFP-Rab7b did not affect vacuole formation in GFP-positive inner cells (Fig. 4 F).

We next investigated whether other Rabs known to function at late endosomes or LROs are necessary for vacuole formation. Rab32 and Rab38 have been shown to regulate post-Golgi trafficking to the melanosome, a LRO (Loftus et al., 2002; Wasmeier et al., 2006; Lopes et al., 2007; Park et al., 2007), and in situ hybridization reveals that *rab32a* is expressed in the notochord at the time of vacuole inflation (Thisse et al., 2001). Therefore, we expressed DN GFP-Rab38b under the control of the *rcn3* promoter and analyzed the effect in transgenic embryos by live confocal microscopy. At 24 hpf, DN GFP-Rab38b did not cause any defects in vacuole formation (Fig. 4 H). In

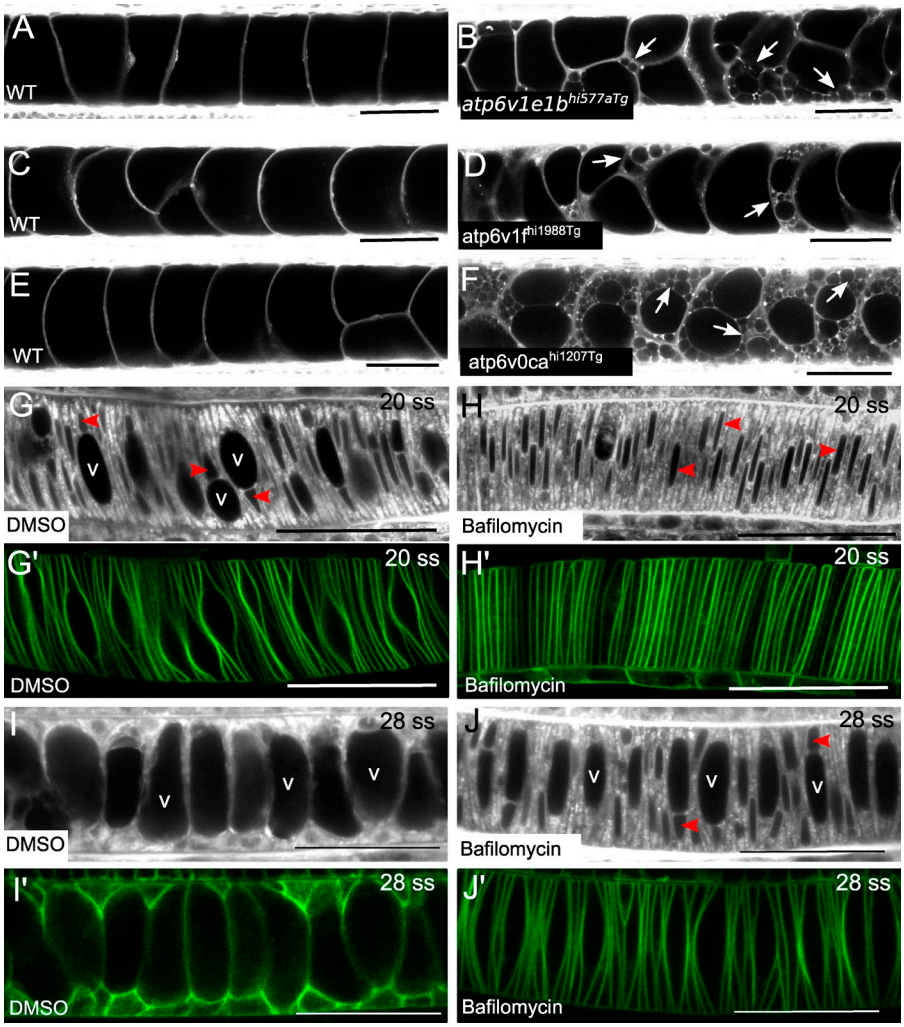

Figure 5. **Notochord vacuoles require vacuolar H⁺-ATPase for formation and maintenance.** (A–F) Live confocal images of 4-dpf WT (A, C, and E) and mutant (B, D, and F) larvae dyed with MED. (B) H⁺-ATPase mutant *atp6v1e1b*^{hi577aTg}. (D) H⁺-ATPase mutant *atp6v1f*^{hi1988Tg}. (F) H⁺-ATPase mutant *atp6v0ca*^{hi1207Tg}. Arrows indicate fragmented vacuoles. (G–H′) Live confocal images of embryos treated with either DMSO or 500 nM bafilomycin for 4 h before vacuole inflation until the 20 ss, visualized with MED (G and H) or membrane GFP (G′ and H′). Live confocal images of embryos treated with either DMSO or 500 nM bafilomycin for 4 h, after vacuole formation had begun, until the 28 ss, visualized with MED (I and J) or membrane GFP (I′ and J′). v labels vacuoles inflating in DMSO control and red arrowheads label nuclei. Bars, 50 µm.

contrast, expression of DN Rab32a caused fragmentation of vacuoles in 90.6% of the expressing cells (n = 32 cells), indicating that Rab32a functions in vacuole formation (Fig. 4 G).

It has been well established that acidity increases within the secretory pathway, from neutral pH in the ER to acidic pH in post-Golgi compartments and lysosomes, and that acidification is required for post-Golgi sorting and trafficking (Mellman, 1992). Because notochord vacuoles use late endosomal machinery and Rab32a, we sought to determine if acidification is necessary for sorting and trafficking to the vacuole. In zebrafish mutant for components of the H⁺-ATPase complex (Nuckels et al., 2009), which drives acidification of intracellular compartments, we assessed vacuole integrity by MED labeling. In *atp6v1e1b*^{hi577aTg}, *atp6v1f*^{hi1988Tg}, and *atp6v0ca*^{hi1207Tg} mutants, notochord vacuoles initially formed, but then fragmented by 3 dpf (Fig. 5, A–F). To test if H⁺-ATPase function is necessary for vacuole formation, embryos were treated with bafilomycin, a potent inhibitor of vacuolar type H⁺-ATPases, before vacuole formation. Embryos expressing notochord-specific GFP-CaaX were treated for 4 h at 15 ss, before the time of vacuole formation, with either 500 nM bafilomycin or DMSO, and incubated in MED. Live confocal imaging revealed that vacuole formation was arrested in bafilomycin-treated embryos (Fig. 5, G and H). We also treated GFP-CaaX embryos after vacuole formation had initiated, from 20 ss until 28 ss, with 500nM bafilomycin or DMSO. Vacuole growth stopped in the bafilomycin-treated embryos, while continuing normally in the DMSO controls (Fig. 5, I and J), indicating that acidification is necessary for vacuole formation. Collectively, these data show that notochord vacuole formation and maintenance requires late endosomal trafficking regulated by Rab32a and H⁺-ATPase–dependent acidification.

The notochord vacuole is a LRO

Because notochord vacuoles use late endosomal and lysosomal machinery as well as Rab32a that is known to traffic to LROs, we investigated whether lysosomal proteins localize to the vacuole (Granger et al., 1990). We generated transgenic fish expressing lysosomal-associated membrane protein 2 (Lamp2) and Lamp1 under the control of a heat shock promoter. Through live confocal imaging, we observed Lamp2-GFP–positive lysosomes within the outer and inner cells of the notochord. Interestingly, Lamp1-RFP labeled punctae within the outer and inner cells as well as the vacuole membrane. Embryos expressing both transgenes showed some colocalizing punctae as well as Lamp1-RFP, but not Lamp2-GFP, on the vacuole membrane (Fig. 6 A).

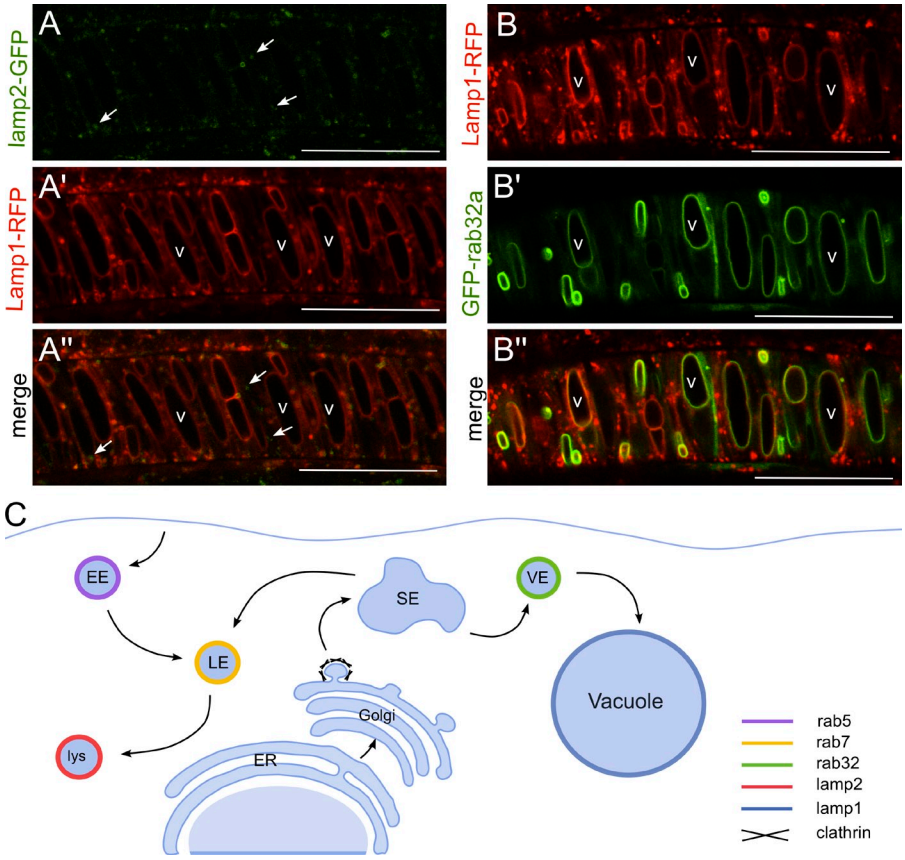

Figure 6. **The notochord vacuole is a unique LRO.** (A, A′, and A′′) Live confocal image of a 20-ss transgenic embryo expressing lamp2-GFP and Lamp1-RFP (*Tg(hsp:lamp2-GFP); Tg(hsp:Lamp1-RFP)*). Lamp expression was induced at 16 ss. Arrows label Lamp2-GFP–positive lysosomes that are not Lamp1-RFP positive. v, vacuoles. (B, B′, and B′′) Live confocal image of a 20-ss transgenic embryo expressing Lamp1-RFP and GFP-Rab32a (*Tg(hsp:Lamp1-RFP); Tg(rcn3:gal4); Tg(UAS:GFP-rab32a)*). Lamp1-RFP expression was induced at 16 ss. v, vacuoles. (C) Cartoon depicting trafficking requirements for vacuole formation. EE, early endosome; LE, late endosome; lys, lysosome; SE, sorting endosome; VE, vacuolar endosome. Bars, 50 µm.

These data show that notochord vacuoles share some characteristics with lysosomes. To test this further, we investigated the subcellular localization of Rab32a. GFP-Rab32a was expressed in transgenic embryos also expressing the vacuole marker Lamp1-RFP in triple transgenic fish—*Tg(rcn3:gal4); Tg(hsp:Lamp1-RFP)*; *Tg(UAS:GFP-rab32a)*. Live confocal imaging at 24 hpf revealed a precise colocalization of GFP-Rab32a with Lamp1-RFP on the vacuole membrane, but not in lysosomes where GFP-Rab32a was absent (Fig. 6 B).

These data indicate that notochord vacuoles are LROs that coexist with lysosomes. However, specific trafficking and sorting is required for cargoes en route to the vacuole versus the lysosome (Fig. 6 C).

Notochord vacuoles are essential for elongation of the embryonic axis

Elegant ex vivo and modeling experiments suggested that the inflation of notochord vacuoles may drive the straightening and elongation of the vertebrate embryo along the rostral-caudal axis (Adams et al., 1990; Koehl et al., 2000). To directly test the role of notochord vacuoles in embryonic zebrafish axis development we targeted vacuole formation and differentiation of the inner and outer cell layers.

Previous work showed that ubiquitous expression of the notch intracellular domain (NICD) during notochord differentiation causes the notochord to adopt an entirely outer sheath cell fate at the expense of the inner cell fate (Yamamoto et al., 2010). To inhibit vacuolated cell differentiation, we expressed NICD in a notochord-specific manner using the *rcn3:gal4* driver (Scheer and Campos-Ortega, 1999). DIC imaging revealed that the majority of the notochord vacuoles failed to form, with only a few vacuoles detectable in the anterior portion of the notochord (Fig. 7 B), a result consistent with previous work (Latimer and Appel, 2006). The body lengths of these larvae were measured from 1 to 5 dpf and compared with nonexpressing siblings (Fig. 7 A). At all time points assessed, NICD-expressing fish were on average 35% shorter than their WT siblings after 1 dpf ($P < 0.0001$ at all time points; $n = 16$ for NICD; $n = 37$ for WT at 5 dpf; Fig. 7 C). Rab5-mediated internalization of the notch receptor is important for proper notch signaling and accumulation of the notch receptor in early endosomes results in increased notch signaling (Vaccari et al., 2008). We analyzed larvae expressing DN mCherry-Rab5c in the notochord before differentiation of inner and outer cell types (Clark et al., 2011). DN mCherry-Rab5–expressing embryos phenocopied embryos expressing NICD and formed very few vacuoles (Fig. 7 E). At 1–5 dpf, DN mCherry-Rab5c fish were on average 18% shorter than their WT siblings ($P < 0.0001$ at all time points; $n = 48$ for DN Rab5c; $n = 84$ for WT at 5 dpf; Fig. 7 F). This defect was only seen when DN mCherry-Rab5c was expressed before differentiation. Expression in the inner cells after differentiation and vacuole formation, using the *SAG214A:gal4* driver, had no effect on vacuole integrity or body axis length ($n = 46$ for DN Rab5c; $n = 49$ for WT at 5 dpf; Fig. 7, G–I).

We next investigated the role of inner cell vacuoles in body axis elongation in a more vacuole-specific manner using a

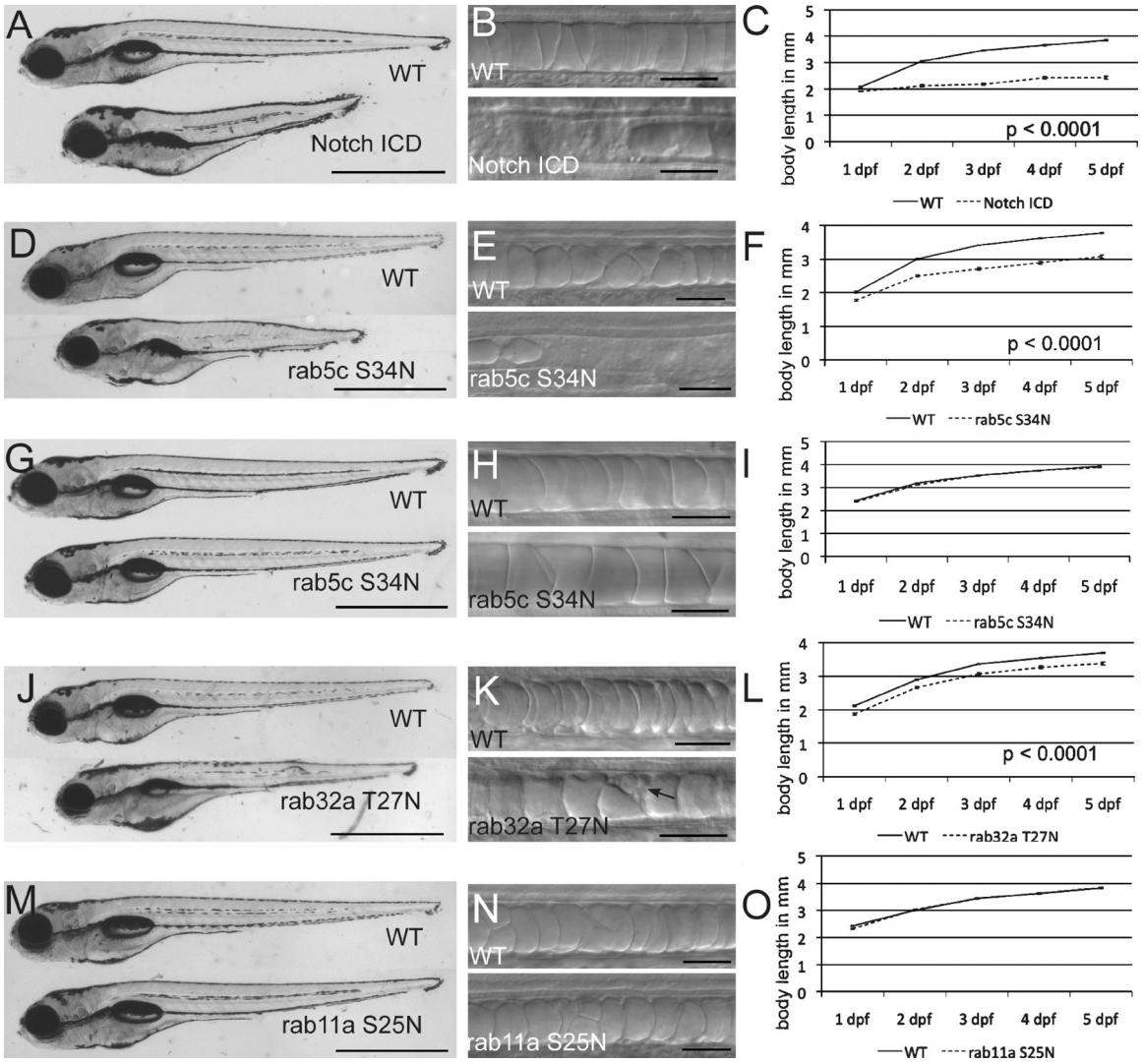

Figure 7. **Notochord vacuoles are required for elongation of the embryonic axis.** (A) Whole-mount image of 5-dpf WT larva expressing NICD in the notochord (*Tg(rcn3:gal4); Tg(UAS:myc-Notch1a-intra)*). (B) Live DIC images of notochords in 48-hpf WT and NICD-expressing larvae. (C) Body length in millimeters from 1 to 5 dpf. $P < 0.0001$ at all time points; $n = 16$ in NICD; $n = 37$ for WT at 5 dpf. (D) Whole-mount image of 5-dpf WT and DN mCherry-Rab5–expressing larvae from the early *rcn3* promoter (*Tg(rcn3:gal4); Tg(UAS:mCherry-rab5c-S34N)*). (E) Live DIC image of 24 hpf WT and DN mCherry-Rab5 notochords. (F) Body length in millimeters from 1 to 5 dpf. $P < 0.0001$ at all time points; $n = 48$ for Rab5cDN; $n = 84$ for WT at 5 dpf. (G) Whole-mount image of 5 dpf WT and DN mCherry-Rab5–expressing larvae from the late *SAG214* driver (*Gt(SAGFF214A:gal4); Tg(UAS:mCherry-rab5c-S34N)*). (H) Live DIC image of 48-hpf WT and rab5cDN notochords. (I) Body length in millimeters from 1 to 5 dpf. No significant difference; $n = 46$ for Rab5cDN; $n = 49$ for WT at 5 dpf. (J) Whole-mount image of 5-dpf transgenic *Tg(rcn3:gal4)* larvae injected with UAS:GFP-rab32a-T27N DNA for mosaic expression. WT is nonexpressing, injected sibling. (K) Live DIC image of 24-hpf WT and DN GFP-Rab32a notochords. Arrow indicates expressing cell with fragmented vacuoles. (L) Body length in millimeters from 1 to 5 dpf. $P < 0.0001$ at all time points; $n = 73$ for Rab32aDN; $n = 84$ for WT at 5 dpf. (M) Whole-mount image of 5-dpf WT and DN mCherry-Rab11a larvae (*Tg(rcn3:gal4); Tg(UAS:mCherry-rab11a-S25N)*). (N) Live DIC image of 24-hpf WT and DN mCherry-Rab11a notochords. (O) Body length in millimeters from 1 to 5 dpf. No significant difference; $n = 54$ for Rab11aDN; $n = 48$ for WT at 5 dpf. Bars: (A, D, G, J, and M) 1 mm; (B, E, H, K, and N) 50 µm. (C, F, I, L, and O) Error bars equal SEM.

mosaic approach. As shown above, in notochord cells expressing DN GFP-Rab32a, vacuoles were fragmented (Fig. 7 K). Fish expressing DN GFP-Rab32a in a mosaic fashion were on average 8% shorter than their WT siblings ($P < 0.0001$ at all time points; $n = 73$ for DN Rab32a; $n = 84$ for WT at 5 dpf; Fig. 7 L). As a control, larvae expressing DN mCherry-Rab11a in the notochord showed no vacuole formation defect and were not significantly shorter than their siblings (Fig. 7, M–O). The same was also seen with DN mCherry-Rab7a (unpublished data).

Thus, when notochord vacuoles are absent or fragmented the body axis is shorter but straight, with normal body curvature. We conclude that notochord vacuoles are required for elongation of the embryonic body axis but not straightening.

Notochord vacuoles are necessary for proper spine morphogenesis

Work in various animal models has shown that notochord cells, including vacuolated cells, become part of the nucleus pulposus within the intervertebral discs as the notochord is

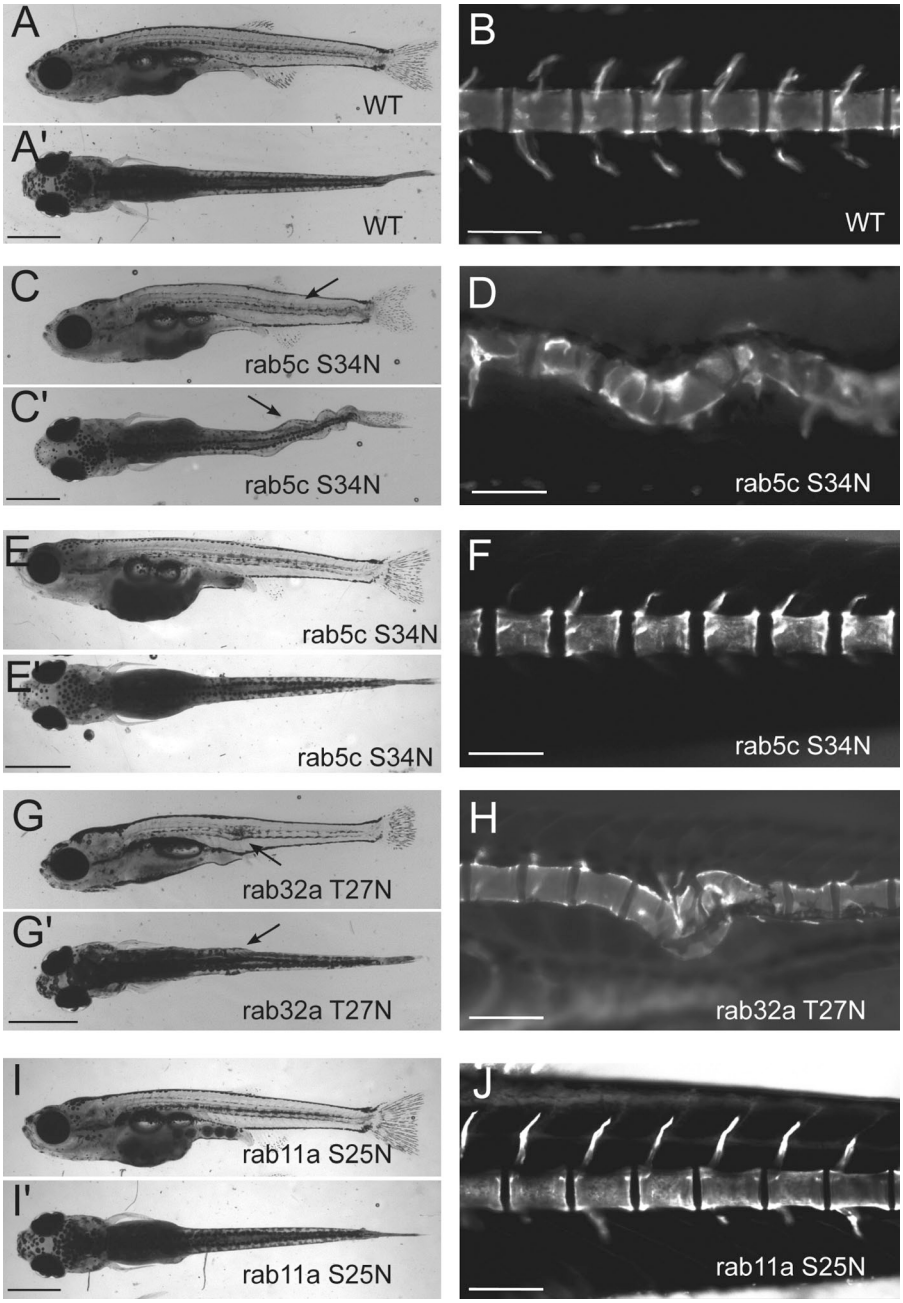

Figure 8. **Notochord vacuoles are necessary for proper spine formation.** (A and A′) Whole-mount image of a 21-dpf WT fish (lateral and dorsal views). (B) Live image of calcein-stained 21-dpf WT spine. (C and C′) Whole-mount image of a 21-dpf DN-mCherry-Rab5c transgenic fish using the early driver *rcn3*; *Tg(rcn3:gal4); Tg(UAS:mCherry-rab5c-S34N)* (lateral and dorsal views). Arrows show body kinks. (D) Live image of calcein-stained 21-dpf spine of a DN mCherry-Rab5c transgenic fish. (E and E′) Whole-mount image of a 21-dpf DN mCherry-Rab5 transgenic fish using the later driver *SAG214A*; *Gt(SAGFF214A:gal4); Tg(UAS:mCherry-rab5c-S34N)* (lateral and dorsal views). (F) Live image of calcein-stained spine of a 21-dpf DN mCherry-Rab5 transgenic fish. (G and G′) Whole-mount image of a 21-dpf mosaic DN GFP-Rab32a fish; *Tg(rcn3:gal4)* embryos injected with UAS:GFP-rab32a-T27N DNA. Lateral and dorsal views are shown; arrows show body kinks. (H) Live image of calcein-stained spine of a 21-dpf DN GFP-Rab32a–expressing fish. (I and I′) Whole-mount image of a 22-dpf transgenic DN mCherry-Rab11a fish (*Tg(rcn3:gal4); Tg(UAS:mCherry-rab11a-S25N)*; lateral and dorsal views). (J) Live image of calcein-stained spine of a 22-dpf DN mCherry-Rab11a transgenic fish. Bars: (A, C, E, G, and I) 1 mm; (B, D, F, H, and J) 200 µm.

replaced by the spine (Walmsley, 1953). We next investigated the role of notochord vacuoles in spine morphogenesis in young juvenile fish. Short larvae without notochord vacuoles were raised for 21 dpf, after which spine morphology was analyzed using the vital dye calcein (Du et al., 2001). In juveniles (21 dpf) that expressed DN mCherry-Rab5c before vacuole differentiation, using the *rcn3* promoter, the body axis appeared straight from a lateral view. In contrast, it was dysmorphic when viewed dorsally (Fig. 8 C). Live imaging with calcein revealed that the spine was severely kinked and wavy with mature and fully formed vertebrae (Fig. 8 D). In contrast, juveniles that expressed DN mCherry-Rab5c after differentiation had normal spines (Fig. 8, E and F). Fish expressing NICD in the notochord fail to inflate their swim bladders and die because they are unable to feed, and therefore could not be analyzed for spine morphogenesis.

To more specifically determine the role of the vacuole in spine morphogenesis, we analyzed fish expressing DN GFP-Rab32a mosaically. *rcn3:gal4* embryos injected with UAS:GFP-rab32a-T27N DNA were raised until 21 dpf and then their spines were visualized with the vital dye calcein. These fish also showed body and spine kinks, although less than fish expressing DN mCherry-Rab5c throughout the notochord (Fig. 8, G and H). Juveniles that expressed DN mCherry-Rab11a, which does not affect the vacuole, showed no body kinks or spine defects (Fig. 8, I and J), indicating that not all DN rabs affect spine formation. These data indentify a novel role for the notochord vacuoles in spine morphogenesis.

Discussion

Here we elucidate the trafficking requirements necessary for vacuole biogenesis and show that post-Golgi trafficking, H^+-ATPase-dependent acidification, and Rab32a function are necessary for formation and maintenance of this specialized structure. Our in vivo studies in zebrafish show that the inflating vacuoles act as a morphogenetic force to elongate the embryonic body axis. Previous ex vivo work had suggested that vacuole inflation could drive both the elongation and straightening of the body axis (Koehl et al., 2000). However, our results show that in vivo vacuole inflation is not required for straightening of the embryonic axis. The expansion of the vacuoles results in the elongation of the embryonic axis longitudinally and not radially, as a result of the rigid ECM surrounding the notochord (Adams et al., 1990; Stemple et al., 1996).

Characterization of the cellular machinery regulating notochord vacuole biogenesis and maintenance uncovered a role for vacuoles in spine morphogenesis. How do vacuoles affect this process? The link between the notochord and vertebral development has been closely examined in Atlantic salmon (Grotmol et al., 2003). There, the ossification of the initial spine structure, the chordacentra, begins within the perinotochordal ECM. Then, mesenchymal cells from the sclerotome invade the notochord and, using the forming chordacentra as a foundation, differentiate into osteoblasts that eventually form the bone matrix of the vertebrae. We hypothesize that the fully inflated vacuoles provide the rigidity necessary to oppose the pushing force of invading osteoblasts during vertebral bone formation. Notochords lacking vacuoles or with fragmented vacuoles are unable to resist these invasive forces, causing kinks in the spine during ossification. Future work will further characterize the role of the vacuole in ossification of the vertebral column.

Recent work in the mouse has implicated notch signaling and hypoxia in scoliosis of the spine by affecting somite patterning through the segmentation clock, thereby affecting spine morphogenesis (Sparrow et al., 2012). However, it is very likely that under those conditions differentiation of the notochord vacuolated cells is also affected and contributes to the overall scoliosis phenotype. The experimental accessibility of the zebrafish notochord will help better understand the link between notochord function and spine morphogenesis shown here.

Many specialized cells contain LROs that are similar to late endosomes or lysosomes and carry out specific functions (Dell'Angelica et al., 2000; Raposo et al., 2007). We propose that the notochord vacuole is a LRO that functions as the main structural component of the notochord. The notochord vacuole, like previously characterized LROs, is a highly specialized post-Golgi structure that requires acidification for its formation, uses the LRO Rab32a, and contains at least one lysosomal membrane protein. However, unlike some LROs, the lumen of the notochord vacuole is not acidic. LysoTracker labeled lysosomes and other internal structures, but not the vacuole lumen in dissected notochords (Fig. S3, A–B). Nevertheless, vacuoles require acidification for their biogenesis and maintenance. We reasoned that the pH gradient generated by the H^+-ATPase may be rapidly dissipated in the vacuole. This could be caused by the presence of basic amino acids in the vacuole or, more likely, by the activity of alkali/H^+ exchangers on the vacuole membrane (Casey et al., 2010). Transport of alkali ions into the vacuole lumen would then drive the movement of water, thereby leading to the swelling of the organelle. In this scenario vacuole integrity should be dependent on the activity of the H^+-ATPase. To test this hypothesis further, we treated dissected notochords from 20 ss embryos with bafilomycin. In agreement with our working model, confocal imaging revealed that after 2 h of incubation with bafilomycin, vacuoles begin to fragment (Fig. S3 C). Future work should identify the ion exchangers on the vacuole membrane and the osmolytes that drive the accumulation of a large volume of water within notochord vacuoles.

Traditionally, it has been assumed that notochord vacuoles contain glycosaminoglycans (GAGs) and that these highly negatively charged molecules may drive vacuole expansion by attracting cations and water (Waddington and Perry, 1962). To determine if GAGs are present in zebrafish notochord vacuoles we generated a secreted GFP that contains a short sequence tag of 10 amino acids (EDEASGIGPE) that is a known GAG attachment site in the proteoglycan decorin (Kobialka et al., 2009). The GAG-tagged GFP (GAG-GFP) was modified and secreted from cells in vitro (Fig. S4 A). In 24-hpf embryos expressing secreted GAG-GFP under the control of the *rcn3* promoter, no GAG-GFP was detected in the vacuole lumen, suggesting that GAGs are not trafficked to the vacuole at this stage (Fig. S4 B). We also checked for the presence of GAGs using immunohistochemistry. Anti-keratan sulfate antibodies labeled the perinotochordal basement membrane as well as the space between the outer sheath layer and inner cell layer but not the lumen of the vacuole (Fig. S4 C). Next, we stained embryos with the basic dye Alcian blue, which labels acidic polysaccharides and mucopolysaccharides, and did not detect any labeling inside the vacuoles (Fig. S4, D and E), suggesting that GAGs are not likely to function as osmolytes within the zebrafish notochord vacuole during embryogenesis.

For many years the vertebrate notochord has been considered an evolutionary relic that only functions in early embryonic development and degenerates shortly thereafter. However, recent work in several vertebrate species has clearly shown that notochord cells persist within the nucleus pulposus of the intervertebral discs (Hunter et al., 2004). This work establishes a continuous structural role for the notochord from embryogenesis until vertebral column formation.

Materials and methods

Fish stocks

Zebrafish stocks were maintained at 28°C and bred as previously described (Westerfield, 2000). A list of zebrafish lines used for this work can be found in Table 1. The *Gt(Gal4FF)nksagff214a* line was a gift from K. Kawakami (National Institute of Genetics, Mishima, Japan). The *Tg(UAS:mCherry-rab5c-S34N)*, *Tg(UAS:mCherry-rab7a-T22N)*, and *Tg(UAS:mCherry-rab11a-S25N)* lines were gifts from B. Link (Medical College of Wisconsin, Milwaukee, WI). The *vps11*$^{wsu1/wsu1}$ line was a gift from R. Thummel (Wayne State University School of Medicine, Detroit, MI). The *atp6v1e1b*$^{hi577aTg/hi577aTg}$, *atp6v1f*$^{hi1988Tg/hi1988Tg}$, and *atp6v0ca*$^{hi1207Tg/hi1207Tg}$ lines were gifts from J. Gross (University of Texas at Austin, Austin, TX). The *Tg(UAS-E1b:6xMYC-notch1a)* line was a gift from S. Kucenas (University of Virginia, Charlottesville, VA).

Table 1. **Transgenic lines used in this paper**

Allele	Genotype	Reference
pd1023	*Tg(rcn3:gal4)*	This work
pd1025	*Tg(UAS:GFP-CaaX)*	This work
pd1009	*Tg(rcn3:GFP-CaaX)*	This work
nksagff214a	*Gt(Gal4FF)nksagff214a*	Yamamoto et al., 2010
hi2462Tg	$cltca^{hi2462Tg/hi2462Tg}$	Amsterdam et al., 2004
mw33	*Tg(UAS:mCherry-rab5c-S34N)*	Clark et al., 2011
wsu1	$vps11^{wsu1/wsu1}$	Thomas et al., 2011
hi2499aTg	$vps18^{hi2499aTg/hi2499aTg}$	Sadler et al., 2005
mw37	*Tg(UAS:mCherry-rab7a-T22N)*	Clark et al., 2011
pd1081	*Tg(UAS:GFP-rab38b-T23N, cmlc2:GFP)*	This work
hi577aTg	$atp6v1e1b^{hi577aTg/hi577aTg}$	Nuckels et al., 2009
hi1988Tg	$atp6v1f^{hi1988Tg/hi1988Tg}$	Nuckels et al., 2009
hi1207Tg	$atp6v0ca^{hi1207Tg/hi1207Tg}$	Nuckels et al., 2009
pd1082	*Tg(hsp:lamp2-GFP)*	This work
pd1064	*Tg(hsp:Lamp1-RFP)*	This work
pd1083	*Tg(UAS:GFP-rab32a, cmlc2:GFP)*	This work
kca3	*Tg(UAS-E1b:6xMYC-notch1a)*	Scheer and Campos-Ortega, 1999
mw35	*Tg(UAS:mCherry-rab11a-S25N)*	Clark et al., 2011
pd1065	*Tg(hsp:RFP-LC3)*	This work
pd1066	*Tg(UAS:s-GFP, cmlc2:GFP)*	This work
pd1067	*Tg(UAS:s-GFP-GAG, cmlc2:GFP)*	This work

Plasmid construction

All constructs for transgenic fish were generated using the Tol2kit gateway cloning system using the p5E-MCS, p5E-hsp70l, pME-MCS, pME-EGFP-CaaX, p3E-polyA, pDestTol2pA2, and pDestTol2CG2 vectors (Kwan et al., 2007). The p5E-4xUAS vector was a gift from M. Goll (Memorial Sloan-Kettering Cancer Center, New York, NY; Akitake et al., 2011). The 1-kb *rcn3* promoter fragment was amplified from genomic DNA using primers with KpnI and HindIII restriction sites: rcn3_KpnI_forward, 5′-GGTACCAACATGACCACGTCAGACCA-3′; and rcn3_HindIII_reverse, 5′-AAGCTTAAGTGTCCCCAGAAAGAGCA-3′. pME-Dyn1-K44A-GFP was generated from Addgene plasmid 22197, pEGFP-N1-human dynamin1aa-K44A (Lee and De Camilli, 2002). pME-Dyn2-K44A-GFP was generated from pEGFP-NI-rat dynamin2aa-K44A (Cook et al., 1994). Rab7b (available from RefSeq under accession no. NM_001002178) was amplified from cDNA using primers with BamHI and NotI restriction sites: rab7b_BamHI_forward, 5′-GGATCCATGGCTTCCCGTAAAAAGGTCCTCC-3′; rab7b_NotI_reverse, 5′-GCGGCCGCTCAGCAGCTGCAGCCTTCACCGTTA-3′. Rab38b was amplified from cDNA using primers with BamHI and NotI restriction sites: rab38b_BamHI_forward, 5′-GGATCCATGCATAACAATCAGAAGGAGCATTTGTAT-3′; and rab38b_NotI_reverse, 5′-GCGGCCGCTCAAGGTTTGAAGCAAGCGGAACAAGT-3′. Rab32a was amplified from cDNA using primers with BglII and NotI restriction sites: rab32a_BglII_forward, 5′-AGATCTATGGCAGGCGGGTCCGTGTCGG-3′; and rab32a_NotI_reverse, 5′-GCGGCCGCCTAGCAGCAACCTGACTTGCTCTC-3′. DN Rab7b, Rab32a, and Rab38b were made using QuikChange II XL site-directed mutagenesis kit (Agilent Technologies). Lamp2 was amplified from cDNA using primers with EcoRI and BamHI restriction sites: lamp2_EcoRI_forward, 5′-GAATTCATGGCTGTCCGCGGTTTTCTGCCTC-3′; and lamp2_BamHI_reverse, 5′-GGATCCCAGTGTCTGATATCCAACATAGGTTCGTCG-3′. pME-Lamp1-RFP was generated from rat Lamp1-RFP (Sherer et al., 2003).

Microscopy

Time-lapse imaging of notochord development, whole-mount live imaging, and fixed section imaging were performed on a confocal microscope (SP5; Leica) with 10×/0.40 HC PL APO air objective, 20×/0.70 HC PL APO oil objective, and 40×/1.25–0.75 HCX PL APO oil objective (all from Leica) and Application Suite software (Leica). Whole-mount live imaging was also performed on a 780 inverted confocal microscope (Carl Zeiss) with 20×/0.8 Dry Plan-Apochromat DIC objective and 40×/1.4 Oil Plan-Apochromat objective (all from Carl Zeiss) and Zen software. Dissected notochord cells were imaged using a 710 inverted confocal microscope (Carl Zeiss) with 63×/1.40 Oil Plan-Apochromat objective (Carl Zeiss) and Zen software. Whole-mount live imaging was also performed on an Axio Imager.M1 microscope with 10×/0.3 EC Plan-NeoFluar objective and 20×/0.8 Plan-Apochromat objective, an AxioCamMRm camera, and AxioVision software (all from Carl Zeiss). Whole-mount live imaging for body length measurements and before calcein dye was performed on a Setero Discovery.V20 microscope with 1.0× Achromat S FWD 63 mm objective, an AxioCamHRc camera, and AxioVision software (all from Carl Zeiss). Where necessary, images were minimally post-processed in ImageJ software (National Institutes of Health) for overall brightness and contrast or to realign channels to correct for drift that occurs during live imaging.

Immunohistochemistry

For cross sections, zebrafish embryos were anesthetized in tricaine solution (Sigma-Aldrich), fixed in 4% PFA overnight, washed several times in PBS, embedded in 4% low melt agarose (GeneMate), and sectioned using a vibratome (VT 1000S; Leica) as previously described (Bagnat et al., 2010). Alexa-568 phalloidin (Invitrogen) was used at 1:500 and sections were mounted on glass slides with Vectashield mounting media containing DAPI (Vector Laboratories). A mouse monoclonal antibody against keratan sulfate (Developmental Studies Hybridoma Bank) was used at 1:100 and detected with Alexa Fluor 488 goat anti–mouse antibody (Molecular Probes) at 1:300.

Pharmacological treatments

BFA (Sigma-Aldrich) was prepared as a 20-mg/ml stock solution in DMSO and used at 5 µg/ml in egg water. Bafilomycin (Sigma-Aldrich) was prepared as a 2-mM stock solution in DMSO and used on fish at 500 nM in egg water and on dissected notochords at 1 µM in L-15 culture media.

Live imaging

The vital dye GFP Counterstain BODIPY TR MED (Molecular Probes) was used for most live imaging. In brief, embryos were soaked in 2% MED for 30 min to 1 h depending on age, rinsed in egg water, mounted on a glass slide in egg water, and imaged immediately. Spines were labeled with the vital dye calcein (Sigma-Aldrich). Fish were incubated in a solution of 0.2% calcein in water for 10 min as previously described (Du et al., 2001), rinsed in fish water, and allowed to rest for 10 min at room temp before mounting in fish water on a slide for imaging. All live imaging was performed at room temperature.

Heat shock

Embryos in egg water were transferred to 50-ml conical tubes and submerged in a 39°C water bath for 30 min to induce *hsp70l* expression.

Dissected notochord assays

Notochords were dissected from fish by incubating embryos in 0.25% trypsin (Gibco) for 5–20 min depending on age. The cell suspension was

passed through a 70-µm cell strainer, and the contents retained in strainer were cultured in L-15 media without phenol red (Gibco) containing 10% fetal bovine serum. For endocytosis assays, FM4-64 dye (Molecular Probes) was prepared as a 4-mM stock solution in water and was cocultured with notochord cells at a final concentration of 4 µM. Dextran Alexa Fluor 568 10,000 MW (Molecular Probes) was prepared as a 5-mg/ml stock and cocultured with notochord cells at a final concentration of 100 µg/ml. LysoTracker red DND-99 (Molecular Probes) comes as a 1-mM stock solution in DMSO and was cocultured with notochord cells at a final concentration of 1 µM. Notochord cells were imaged in L-15 culture media without phenol red containing 10% fetal bovine serum in 35-mm glass bottom microwell dishes at room temperature.

Body length measurements

Fish were mounted in 2% methylcellulose for whole-mount imaging and then recovered. Body length was measured from the tip of the nose to the tip of the tail using ImageJ software.

Western blot

HEK293AD cells were transfected with pcDNA3-s-RFP or pcDNA3-s-GFP-GAG using Lipofectamine 2000 (Invitrogen). Cells were allowed to secrete into media for 3 d and then supernatants were collected. Samples were spun for 5 min at 1,500 to pellet any cellular debris and the supernatant was removed. Laemmli sample buffer was added to supernatant and cells and boiled for 5 min, and samples were loaded into SDS-PAGE gels. Secreted RFP was detected with rabbit polyclonal anti-DS red antibody (Takara Bio Inc.) at 1:1,000 and secreted GFP-GAG was detected with rabbit polyclonal anti-GFP antibody (AnaSpec).

Alcian blue

GAGs were labeled with Alcian blue as previously described (Neuhauss et al., 1996). In brief, embryos were fixed in 4% PFA overnight and washed several times in PBS. Embryos were bleached in 30% hydrogen peroxide until the eyes were translucent. Embryos were rinsed in PBS and transferred to Alcian blue solution overnight (70% EtOH, 1% HCl, and 0.1% Alcian blue). Embryos were cleared in acidic ethanol (70% EtOH and 5% HCl) until clear.

Online supplemental material

Fig. S1 illustrates that the promoter *rcn3* turns on at 6 ss in transgenic embryos expressing GFP-CaaX. Fig. S2 shows that GFP secreted from cells in vitro and in vivo does not accumulate in the notochord vacuoles. Fig. S3 shows that LysoTracker red does not accumulate in the vacuole in dissected notochord cells and that bafilomycin causes the vacuole to fragment in dissected notochord cells. Fig. S4 shows that a GAG-tagged GFP secreted from cells in vitro and in vivo is not trafficking to the notochord vacuoles. A keratan sulfate antibody and Alcian blue staining confirm that there are no GAGs in the lumen of the vacuoles. Online supplemental material is available at http://www.jcb.org/cgi/content/full/jcb.201212095/DC1. Additional data are available in the JCB DataViewer at http://dx.doi.org/10.1083/jcb.201212095.dv.

We would like to thank the Zebrafish Facility and Light Microscopy Core Facility at Duke University. We also thank members of the Bagnat laboratory for helpful advice and discussions regarding this work. We thank Koichi Kawakami, Brian Link, Ryan Thummel, Jeff Gross, John Rawls, and Sarah Kucenas for fish lines. The 3H1 monoclonal keratan sulfate antibody was obtained from the Developmental Studies Hybridoma Bank developed under the auspices of the National Institute of Child Health and Human Development and maintained by The University of Iowa. We also thank Cagla Eroglu, Ken Poss, Terry Lechler, and Chris Nicchitta for critical reading of this manuscript.

This work was funded by a National Institutes of Health innovator grant (1DP2OD006486) to M. Bagnat.

Submitted: 17 December 2012
Accepted: 5 February 2013

References

Adams, D.S., R. Keller, and M.A. Koehl. 1990. The mechanics of notochord elongation, straightening and stiffening in the embryo of *Xenopus laevis*. *Development*. 110:115–130.

Akitake, C.M., M. Macurak, M.E. Halpern, and M.G. Goll. 2011. Transgenerational analysis of transcriptional silencing in zebrafish. *Dev. Biol.* 352: 191–201. http://dx.doi.org/10.1016/j.ydbio.2011.01.002

Amsterdam, A., R.M. Nissen, Z. Sun, E.C. Swindell, S. Farrington, and N. Hopkins. 2004. Identification of 315 genes essential for early zebrafish development. *Proc. Natl. Acad. Sci. USA*. 101:12792–12797. http://dx.doi.org/10.1073/pnas.0403929101

Anderson, R.G., J.L. Goldstein, and M.S. Brown. 1977. A mutation that impairs the ability of lipoprotein receptors to localise in coated pits on the cell surface of human fibroblasts. *Nature*. 270:695–699. http://dx.doi.org/10.1038/270695a0

Bagnat, M., A. Navis, S. Herbstreith, K. Brand-Arzamendi, S. Curado, S. Gabriel, K. Mostov, J. Huisken, and D.Y. Stainier. 2010. Cse1l is a negative regulator of CFTR-dependent fluid secretion. *Curr. Biol.* 20:1840–1845. http://dx.doi.org/10.1016/j.cub.2010.09.012

Bancroft, M., and R. Bellairs. 1976. The development of the notochord in the chick embryo, studied by scanning and transmission electron microscopy. *J. Embryol. Exp. Morphol.* 35:383–401.

Casey, J.R., S. Grinstein, and J. Orlowski. 2010. Sensors and regulators of intracellular pH. *Nat. Rev. Mol. Cell Biol.* 11:50–61. http://dx.doi.org/10.1038/nrm2820

Chen, M.S., R.A. Obar, C.C. Schroeder, T.W. Austin, C.A. Poodry, S.C. Wadsworth, and R.B. Vallee. 1991. Multiple forms of dynamin are encoded by shibire, a *Drosophila* gene involved in endocytosis. *Nature*. 351:583–586. http://dx.doi.org/10.1038/351583a0

Choi, K.S., C. Lee, and B.D. Harfe. 2012. Sonic hedgehog in the notochord is sufficient for patterning of the intervertebral discs. *Mech. Dev.* 129:255–262. http://dx.doi.org/10.1016/j.mod.2012.07.003

Clark, B.S., M. Winter, A.R. Cohen, and B.A. Link. 2011. Generation of Rab-based transgenic lines for in vivo studies of endosome biology in zebrafish. *Dev. Dyn.* 240:2452–2465. http://dx.doi.org/10.1002/dvdy.22758

Cook, T.A., R. Urrutia, and M.A. McNiven. 1994. Identification of dynamin 2, an isoform ubiquitously expressed in rat tissues. *Proc. Natl. Acad. Sci. USA*. 91:644–648. http://dx.doi.org/10.1073/pnas.91.2.644

Coutinho, P., M.J. Parsons, K.A. Thomas, E.M. Hirst, L. Saúde, I. Campos, P.H. Williams, and D.L. Stemple. 2004. Differential requirements for COPI transport during vertebrate early development. *Dev. Cell*. 7:547–558. http://dx.doi.org/10.1016/j.devcel.2004.07.020

Dale, R.M., and J. Topczewski. 2011. Identification of an evolutionarily conserved regulatory element of the zebrafish col2a1a gene. *Dev. Biol.* 357:518–531. http://dx.doi.org/10.1016/j.ydbio.2011.06.020

Deborde, S., E. Perret, D. Gravotta, A. Deora, S. Salvarezza, R. Schreiner, and E. Rodriguez-Boulan. 2008. Clathrin is a key regulator of basolateral polarity. *Nature*. 452:719–723. http://dx.doi.org/10.1038/nature06828

Dell'Angelica, E.C., C. Mullins, S. Caplan, and J.S. Bonifacino. 2000. Lysosome-related organelles. *FASEB J.* 14:1265–1278. http://dx.doi.org/10.1096/fj.14.10.1265

Du, S.J., V. Frenkel, G. Kindschi, and Y. Zohar. 2001. Visualizing normal and defective bone development in zebrafish embryos using the fluorescent chromophore calcein. *Dev. Biol.* 238:239–246. http://dx.doi.org/10.1006/dbio.2001.0390

Fouquet, B., B.M. Weinstein, F.C. Serluca, and M.C. Fishman. 1997. Vessel patterning in the embryo of the zebrafish: guidance by notochord. *Dev. Biol.* 183:37–48. http://dx.doi.org/10.1006/dbio.1996.8495

Glickman, N.S., C.B. Kimmel, M.A. Jones, and R.J. Adams. 2003. Shaping the zebrafish notochord. *Development*. 130:873–887. http://dx.doi.org/10.1242/dev.00314

Granger, B.L., S.A. Green, C.A. Gabel, C.L. Howe, I. Mellman, and A. Helenius. 1990. Characterization and cloning of lgp110, a lysosomal membrane glycoprotein from mouse and rat cells. *J. Biol. Chem.* 265: 12036–12043.

Griffin, K.J., and D. Kimelman. 2003. Interplay between FGF, one-eyed pinhead, and T-box transcription factors during zebrafish posterior development. *Dev. Biol.* 264:456–466. http://dx.doi.org/10.1016/j.ydbio.2003.09.008

Grotmol, S., H. Kryvi, K. Nordvik, and G.K. Totland. 2003. Notochord segmentation may lay down the pathway for the development of the vertebral bodies in the Atlantic salmon. *Anat. Embryol. (Berl.)*. 207:263–272. http://dx.doi.org/10.1007/s00429-003-0349-y

Herskovits, J.S., C.C. Burgess, R.A. Obar, and R.B. Vallee. 1993. Effects of mutant rat dynamin on endocytosis. *J. Cell Biol.* 122:565–578. http://dx.doi.org/10.1083/jcb.122.3.565

Hunter, C.J., J.R. Matyas, and N.A. Duncan. 2004. Cytomorphology of notochordal and chondrocytic cells from the nucleus pulposus: a species comparison. *J. Anat.* 205:357–362. http://dx.doi.org/10.1111/j.0021-8782.2004.00352.x

Hunter, C.J., S. Bianchi, P. Cheng, and K. Muldrew. 2007. Osmoregulatory function of large vacuoles found in notochordal cells of the intervertebral disc. *Mol. Cell. Biomech.* 4:227–237.

Kida, Y.S., T. Sato, K.Y. Miyasaka, A. Suto, and T. Ogura. 2007. Daam1 regulates the endocytosis of EphB during the convergent extension of the

zebrafish notochord. *Proc. Natl. Acad. Sci. USA*. 104:6708–6713. http://dx.doi.org/10.1073/pnas.0608946104

Kim, S.K., M. Hebrok, and D.A. Melton. 1997. Notochord to endoderm signaling is required for pancreas development. *Development*. 124:4243–4252.

Kobialka, S., N. Beuret, H. Ben-Tekaya, and M. Spiess. 2009. Glycosaminoglycan chains affect exocytic and endocytic protein traffic. *Traffic*. 10:1845–1855. http://dx.doi.org/10.1111/j.1600-0854.2009.00987.x

Koehl, M.A., K.J. Quillin, and C.A. Pell. 2000. Mechanical design of fiber-wound hydraulic skeletons: the stiffening and straightening of embryonic notochords. *Am. Zool.* 40:28–41. http://dx.doi.org/10.1668/0003-1569(2000)040[0028:MDOFWH]2.0.CO;2

Kreitzer, G., A. Marmorstein, P. Okamoto, R. Vallee, and E. Rodriguez-Boulan. 2000. Kinesin and dynamin are required for post-Golgi transport of a plasma-membrane protein. *Nat. Cell Biol.* 2:125–127. http://dx.doi.org/10.1038/35000081

Kwan, K.M., E. Fujimoto, C. Grabher, B.D. Mangum, M.E. Hardy, D.S. Campbell, J.M. Parant, H.J. Yost, J.P. Kanki, and C.B. Chien. 2007. The Tol2kit: a multisite gateway-based construction kit for Tol2 transposon transgenesis constructs. *Dev. Dyn.* 236:3088–3099. http://dx.doi.org/10.1002/dvdy.21343

Latimer, A.J., and B. Appel. 2006. Notch signaling regulates midline cell specification and proliferation in zebrafish. *Dev. Biol.* 298:392–402. http://dx.doi.org/10.1016/j.ydbio.2006.05.039

Lee, E., and P. De Camilli. 2002. Dynamin at actin tails. *Proc. Natl. Acad. Sci. USA*. 99:161–166. http://dx.doi.org/10.1073/pnas.012607799

Leeson, T.S., and C.R. Leeson. 1958. Observations on the histochemistry and fine structure of the notochord in rabbit embryos. *J. Anat.* 92:278–285.

Lippincott-Schwartz, J., L.C. Yuan, J.S. Bonifacino, and R.D. Klausner. 1989. Rapid redistribution of Golgi proteins into the ER in cells treated with brefeldin A: evidence for membrane cycling from Golgi to ER. *Cell*. 56:801–813. http://dx.doi.org/10.1016/0092-8674(89)90685-5

Loftus, S.K., D.M. Larson, L.L. Baxter, A. Antonellis, Y. Chen, X. Wu, Y. Jiang, M. Bittner, J.A. Hammer III, and W.J. Pavan. 2002. Mutation of melanosome protein RAB38 in chocolate mice. *Proc. Natl. Acad. Sci. USA*. 99:4471–4476. http://dx.doi.org/10.1073/pnas.072087599

Lopes, V.S., C. Wasmeier, M.C. Seabra, and C.E. Futter. 2007. Melanosome maturation defect in Rab38-deficient retinal pigment epithelium results in instability of immature melanosomes during transient melanogenesis. *Mol. Biol. Cell*. 18:3914–3927. http://dx.doi.org/10.1091/mbc.E07-03-0268

McCann, M.R., O.J. Tamplin, J. Rossant, and C.A. Séguin. 2012. Tracing notochord-derived cells using a Noto-cre mouse: implications for intervertebral disc development. *Dis. Model. Mech.* 5:73–82. http://dx.doi.org/10.1242/dmm.008128

Meachim, G., and M.S. Cornah. 1970. Fine structure of juvenile human nucleus pulposus. *J. Anat.* 107:337–350.

Mellman, I. 1992. The importance of being acid: the role of acidification in intracellular membrane traffic. *J. Exp. Biol.* 172:39–45.

Melville, D.B., M. Montero-Balaguer, D.S. Levic, K. Bradley, J.R. Smith, A.K. Hatzopoulos, and E.W. Knapik. 2011. The feelgood mutation in zebrafish dysregulates COPII-dependent secretion of select extracellular matrix proteins in skeletal morphogenesis. *Dis. Model. Mech.* 4:763–776. http://dx.doi.org/10.1242/dmm.007625

Neuhauss, S.C., L. Solnica-Krezel, A.F. Schier, F. Zwartkruis, D.L. Stemple, J. Malicki, S. Abdelilah, D.Y. Stainier, and W. Driever. 1996. Mutations affecting craniofacial development in zebrafish. *Development*. 123:357–367.

Nuckels, R.J., A. Ng, T. Darland, and J.M. Gross. 2009. The vacuolar-ATPase complex regulates retinoblast proliferation and survival, photoreceptor morphogenesis, and pigmentation in the zebrafish eye. *Invest. Ophthalmol. Vis. Sci.* 50:893–905. http://dx.doi.org/10.1167/iovs.08-2743

Odenthal, J., P. Haffter, E. Vogelsang, M. Brand, F.J. van Eeden, M. Furutani-Seiki, M. Granato, M. Hammerschmidt, C.P. Heisenberg, Y.J. Jiang, et al. 1996. Mutations affecting the formation of the notochord in the zebrafish, *Danio rerio*. *Development*. 123:103–115.

Park, M., A.S. Serpinskaya, N. Papalopulu, and V.I. Gelfand. 2007. Rab32 regulates melanosome transport in *Xenopus* melanophores by protein kinase a recruitment. *Curr. Biol.* 17:2030–2034. http://dx.doi.org/10.1016/j.cub.2007.10.051

Pourquié, O., M. Coltey, M.A. Teillet, C. Ordahl, and N.M. Le Douarin. 1993. Control of dorsoventral patterning of somitic derivatives by notochord and floor plate. *Proc. Natl. Acad. Sci. USA*. 90:5242–5246. http://dx.doi.org/10.1073/pnas.90.11.5242

Raposo, G., M.S. Marks, and D.F. Cutler. 2007. Lysosome-related organelles: driving post-Golgi compartments into specialisation. *Curr. Opin. Cell Biol.* 19:394–401. http://dx.doi.org/10.1016/j.ceb.2007.05.001

Raymond, C.K., I. Howald-Stevenson, C.A. Vater, and T.H. Stevens. 1992. Morphological classification of the yeast vacuolar protein sorting mutants: evidence for a prevacuolar compartment in class E vps mutants. *Mol. Biol. Cell*. 3:1389–1402.

Sadler, K.C., A. Amsterdam, C. Soroka, J. Boyer, and N. Hopkins. 2005. A genetic screen in zebrafish identifies the mutants vps18, nf2 and foie gras as models of liver disease. *Development*. 132:3561–3572. http://dx.doi.org/10.1242/dev.01918

Saúde, L., K. Woolley, P. Martin, W. Driever, and D.L. Stemple. 2000. Axis-inducing activities and cell fates of the zebrafish organizer. *Development*. 127:3407–3417.

Scheer, N., and J. Campos-Ortega. 1999. Use of the Gal4-UAS technique for targeted gene expression in the zebrafish. *Mech. Dev.* 80:153–158.

Schmidt, J., V. Francois, E. Bier, and D. Kimelman. 1995. *Drosophila* short gastrulation induces an ectopic axis in *Xenopus*: evidence for conserved mechanisms of dorsal-ventral patterning. *Development*. 121:4319–4328.

Sepich, D.S., C. Calmelet, M. Kiskowski, and L. Solnica-Krezel. 2005. Initiation of convergence and extension movements of lateral mesoderm during zebrafish gastrulation. *Dev. Dyn.* 234:279–292. http://dx.doi.org/10.1002/dvdy.20507

Sherer, N.M., M.J. Lehmann, L.F. Jimenez-Soto, A. Ingmundson, S.M. Horner, G. Cicchetti, P.G. Allen, M. Pypaert, J.M. Cunningham, and W. Mothes. 2003. Visualization of retroviral replication in living cells reveals budding into multivesicular bodies. *Traffic*. 4:785–801. http://dx.doi.org/10.1034/j.1600-0854.2003.00135.x

Shih, J., and S.E. Fraser. 1996. Characterizing the zebrafish organizer: microsurgical analysis at the early-shield stage. *Development*. 122:1313–1322.

Sparrow, D.B., G. Chapman, A.J. Smith, M.Z. Mattar, J.A. Major, V.C. O'Reilly, Y. Saga, E.H. Zackai, J.P. Dormans, B.A. Alman, et al. 2012. A mechanism for gene-environment interaction in the etiology of congenital scoliosis. *Cell*. 149:295–306.

Stemple, D.L., L. Solnica-Krezel, F. Zwartkruis, S.C. Neuhauss, A.F. Schier, J. Malicki, D.Y. Stainier, S. Abdelilah, Z. Rangini, E. Mountcastle-Shah, and W. Driever. 1996. Mutations affecting development of the notochord in zebrafish. *Development*. 123:117–128.

Thisse, B., S. Pfumio, M. Furthauer, B. Loppin, V. Heyer, A. Degrave, R. Woehl, A. Lux, T. Steffan, X.Q. Charbonnier, and C. Thisse. 2001. Expression of the zebrafish genome during embryogenesis. *ZFIN online publication*. http://zfin.org/cgi-bin/webdriver?MIval=aa-pubview2.apg&OID=ZDB-PUB-010810-1 (accessed December 10, 2012).

Thomas, J.L., T.S. Vihtelic, A.D. denDekker, G. Willer, X. Luo, T.R. Murphy, R.G. Gregg, D.R. Hyde, and R. Thummel. 2011. The loss of vacuolar protein sorting 11 (vps11) causes retinal pathogenesis in a vertebrate model of syndromic albinism. *Invest. Ophthalmol. Vis. Sci.* 52:3119–3128. http://dx.doi.org/10.1167/iovs.10-5957

Vaccari, T., H. Lu, R. Kanwar, M.E. Fortini, and D. Bilder. 2008. Endosomal entry regulates Notch receptor activation in *Drosophila melanogaster*. *J. Cell Biol.* 180:755–762. http://dx.doi.org/10.1083/jcb.200708127

Waddington, C.H., and M.M. Perry. 1962. The ultrastructure of the developing urodele notochord. *Proc. R. Soc. Lond. B Biol. Sci.* 156:459–482. http://dx.doi.org/10.1098/rspb.1962.0050

Walmsley, R. 1953. The development and growth of the intervertebral disc. *Edinburgh Med. J.* 60:341–364.

Wasmeier, C., M. Romao, L. Plowright, D.C. Bennett, G. Raposo, and M.C. Seabra. 2006. Rab38 and Rab32 control post-Golgi trafficking of melanogenic enzymes. *J. Cell Biol.* 175:271–281. http://dx.doi.org/10.1083/jcb.200606050

Westerfield, M. 2000. The Zebrafish Book. A guide for the laboratory use of zebrafish (*Danio rerio*). University of Oregon Press, Eugene, OR. 307 pp.

Yamada, T., M. Placzek, H. Tanaka, J. Dodd, and T.M. Jessell. 1991. Control of cell pattern in the developing nervous system: polarizing activity of the floor plate and notochord. *Cell*. 64:635–647. http://dx.doi.org/10.1016/0092-8674(91)90247-V

Yamada, T., S.L. Pfaff, T. Edlund, and T.M. Jessell. 1993. Control of cell pattern in the neural tube: motor neuron induction by diffusible factors from notochord and floor plate. *Cell*. 73:673–686. http://dx.doi.org/10.1016/0092-8674(93)90248-O

Yamamoto, M., R. Morita, T. Mizoguchi, H. Matsuo, M. Isoda, T. Ishitani, A.B. Chitnis, K. Matsumoto, J.G. Crump, K. Hozumi, et al. 2010. Mib-Jag1-Notch signalling regulates patterning and structural roles of the notochord by controlling cell-fate decisions. *Development*. 137:2527–2537. http://dx.doi.org/10.1242/dev.051011